IEEE Access
Multidisciplinary : Rapid Review : Open Access Journal

Received November 6, 2019, accepted December 3, 2019, date of publication December 18, 2019, date of current version December 30, 2019.

Digital Object Identifier 10.1109/ACCESS.2019.2960394

Spatial Averaging Schemes of *In Situ* Electric Field for Low-Frequency Magnetic Field Exposures

YINLIANG DIAO[1,2], (Member, IEEE), JOSE GOMEZ-TAMES[1], (Member, IEEE), ESSAM A. RASHED[1,3,4], (Senior Member, IEEE), ROBERT KAVET[5], (Senior Member, IEEE), AND AKIMASA HIRATA[1,6], (Fellow, IEEE)

[1]Department of Electrical and Mechanical Engineering, Nagoya Institute of Technology, Nagoya 466-8555, Japan
[2]College of Electronic Engineering, South China Agricultural University, Guangzhou 510642, China
[3]Department of Computer Science, Faculty of Informatics and Computer Science, The British University in Egypt, Cairo 11837, Egypt
[4]Department of Mathematics, Faculty of Science, Suez Canal University, Ismailia 41522, Egypt
[5]Kavet Consulting LLC, Oakland, CA 94619, USA
[6]Center of Biomedical Physics and Information Technology, Nagoya Institute of Technology, Nagoya 466-8555, Japan

Corresponding authors: Yinliang Diao (diaoyinliang@ieee.org) and Akimasa Hirata (ahirata@nitech.ac.jp)

This work was supported by the Ministry of Internal Affairs and Communications, Japan.

ABSTRACT ICNIRP and IEEE publish standards/guidelines for exposures to low-frequency electromagnetic fields and their associated *in situ* electric fields. Two methods are prescribed for spatially averaging the *in situ* electric field to evaluate compliance: averaging (1) over a 2 mm × 2 mm × 2 mm volume (ICNIRP) and (2) along a 5 mm linear segment of neural tissue (IEEE). However, detailed calculation procedures for these two schemes are not provided, particularly when the averaging volume/line straddles a tissue/air or tissue/tissue interface. This study proposes detailed schemes for implementing the volume- and line-averaging in such cases, applying them to both a spherical model of layered tissues and a human anatomical model. To extend the applicability of the proposed averaging schemes to the voxels at the tissue boundaries, a parameter, $p_{\max}$, is introduced and defined as the maximum permissible percentage of air/other tissues in the averaging volume/line. For most inner-tissue voxels results show good agreement between the two averaging schemes, in general. Excluding skin, the relative differences between the two averaging schemes were less than 9% for the 99$^{\text{th}}$ percentile *in situ* electric field, and these differences decrease as $p_{\max}$ increases. Results indicate that around 20-30% inclusion of air or other tissues for volume averaging of internal tissues provides stable percentile values; less stability is observed across $p_{\max}$ for linear averaging. Invoking the suggestion of ICNIRP (2010) that the averaging cube for skin "*may extend to subcutaneous tissue*," ≥10% inclusion of air results in stable averaged induced electric fields.

INDEX TERMS Human safety, dosimetry, standardization, low frequency, spatial averaging.

I. INTRODUCTION

Limits for exposures to non-ionizing electromagnetic fields (EMF) from 0-300 GHz and contact currents from 0-110 MHz have been developed and published by the International Commission on Non-Ionizing Radiation Protection (ICNIRP) [1], [2] and by the IEEE International Committee on Electromagnetic Safety (IEEE ICES) Technical Committee 95 [3], [4]. For convenience this paper refers to these guidelines/standards as *guidelines*, the term used by ICNIRP, although IEEE applies the term *standard*.

ICNIRP defines the lower frequency range as <10 MHz, while the IEEE's is <5 MHz. In a general sense, both aim to protect against magnetic-field-coupled stimulation of excitable tissue both in the central nervous system (CNS) and peripherally. Despite this mutual similarity, their specific approaches and specific quantitative limits differ on a number of counts [5]–[7]. Both guidelines specify not-to-be-exceeded *in situ* electric fields in target tissue for exposure to an external magnetic field. ICNIRP calls the *in situ* limit the *basic restriction* (BR), and IEEE's equivalent term is the *dosimetric reference limit* (DRL). The limits established for environmental exposures – *reference levels* (RL) for ICNIRP and *exposure reference levels* (ERL) for IEEE – are derived such that compliance with them assures that the BR and DRL are not exceeded. ICNIRP's limits are classified either for the general public or for *occupational exposure*, with less conservative limits for the latter. IEEE divides exposure

The associate editor coordinating the review of this manuscript and approving it for publication was Flavia Grassi.

scenarios into either *restricted* or *unrestricted* environments, with the restricted environment denoting a location with the possibility of exceeding the unrestricted DRL.

ICNIRP addresses peripheral nerve stimulation (PNS) for frequencies >300 Hz for the general public and >400 Hz for occupational exposure; IEEE's ERLs protect against adverse PNS for frequencies >~750 Hz for all environments. Below these frequencies the guidelines protect against adverse effects in the CNS. ICNIRP's guideline cites transient effects on "*brain functions such as visual processing and motor co-ordination*" based on indirect evidence, with IEEE identifying "*synaptic activity alteration*" as the undesired effect. Clearly, given these differences, there is a "*grey-area*" frequency range (~300-750 Hz) within which the target tissue for deriving RLs and ERLs transitions from CNS to peripheral nerve.

The criteria dose for evaluating BR compliance is defined by ICNIRP "*as a vector average of the electric field in a small contiguous tissue volume of 2 ×2×2 mm*^{3}. *For a specific tissue, the 99*th *percentile value of the electric field is the relevant value to be compared with the basic restriction*." This approach was selected "*as a practical compromise, satisfying requirements for a sound biological basis and computational constraints*." A "*small-volume*" approach would appear to be more appropriate for evaluating BR exceedances in the CNS, as complex networks of synaptic and dendritic connections occupy small volumes [8], whereas PNS results from electric field gradients parallel to the axon.

For IEEE, "*the in situ electric field DRL applies to the rms electric field strength measured in the direction and location providing the maximum in situ electric field vector (vector magnitude) over a* 5 *mm linear distance.*" The latter does not specify a percentile because the underlying dosimetry is based on closed form solutions of uniform isotropic ellipsoidal induction models. The 5-mm IEEE criterion was derived from the length of exposed myelinated nerve in an *in situ* electric field needed to trigger an action potential [9], and thus may not be ideally applicable to predicting altered synaptic activity in the CNS.

These discrepancies have been detailed by Reilly and Hirata in the context of the IEEE-ICES research agenda [5], and several working groups have been established to resolve related issues [10]–[12]. Future revisions to the IEEE-ICES standard will more than likely adopt dosimetry with anatomically realistic models, and considerations of percentile *in situ* electric fields will then be necessary.

Many studies [13]–[25] have reported the relationship between the external magnetic field and the *in situ* electric field coupled into tissue, with other analyses comparing results among different laboratories [26]–[28]. Historically, the 99$^{\text{th}}$ percentile value of the current density or *in situ* electric field was introduced to exclude computational artefacts [29], [30]. In low-frequency dosimetry, artefacts may include i) segmentation error in an anatomical model, which may include the quality of medical images acquired in millimeter resolution [31], ii) discretization error in modeling tissue with a finite grid resolution [32], and iii) potential error in the computations themselves, which may also partly originate in discretization error [33].

The 99$^{\text{th}}$ percentile value of the *in situ* electric field is acceptable (and possibly conservative) when the magnetic field is uniform across a tissue situated within a confined volume (e.g., heart, liver, kidney) [29], [30]. However, it may be inappropriate for localized exposure to distributed tissue (e.g., skin, fat, peripheral nerve), in which the 99$^{\text{th}}$ percentile across the entire distributed tissue would produce underestimates of the relevant dose to the localized site [11].

Several techniques have been proposed to avoid underestimation of dose for localized exposures [11], [34], and may be classified as pre- or post-processing. Examples include a conductivity-smoothing algorithm was introduced before the numerical calculation of *in situ* electric field [34], and an outlier removal method based on the frequency distribution of the highest 1% electric field strengths was proposed in [11]. However, these techniques are not adequately resolved for cases in which the prescribed averaging dimensions cross a tissue/tissue or a tissue/air interface. Specifically, ICNIRP and IEEE specify that the averaging volume or linear segment should not extend beyond the targeted tissue surface. However, this can exclude voxels (or line segments) that include the tissue boundary. The objective of this paper is to use post-processing techniques to quantify the permissible maximum fraction of such voxels or line segments that can be included in a computation without introducing unacceptable artefact. The analyses compare the cubic and linear averaging schemes, and the influence of the adjacent tissue or air beyond the tissue boundary are investigated using a multi-layered sphere and a detailed anatomical human model, each with a range of spatial resolutions.

II. COMPUTATIONAL METHODS AND HUMAN MODEL

A. ELECTROMAGNETIC ANALYSIS

At frequencies up to ~10 MHz, the human body is assumed to not perturb the external magnetic field [35]. Also, by ignoring propagation, capacitive, and inductive effects, Maxwell's equations are simplified with the quasi-static approximation [35]–[37]. The resulting electric scalar potentials for an external magnetic field are computed using the scalar-potential finite difference method:

$$\nabla \cdot [\sigma(-\nabla\varphi - \mathrm{j}\omega \boldsymbol{A}_0)] = 0, \quad (1)$$

where $\boldsymbol{A}_0$ and σ denote the magnetic vector potential of the applied magnetic field and the tissue conductivity, respectively. In this study, the scalar potential is computed iteratively via the successive-over-relaxation and multigrid methods [38]. When (1) is solved, the *in situ* electric field $\boldsymbol{E}$ is calculated as: $\boldsymbol{E} = -\nabla\varphi - \mathrm{j}\omega\boldsymbol{A}_0$.

B. SPHERICAL/ANATOMICAL MODELS AND EXPOSURE SCENRIOS

A multi-layer sphere exposed to a uniform magnetic field is considered. As shown in Fig. 1 (a), the multi-layer sphere

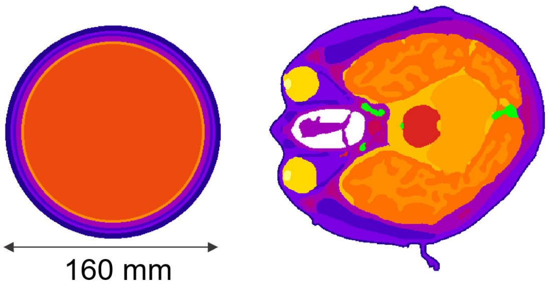

FIGURE 1. Transverse sections of (a) multi-layer spherical model and (b) TARO model at eye level.

TABLE 1. Human tissue conductivities of TARO head model.

Tissue	Conductivity at 50 Hz (S/m)	Color Label
Skin	0.10	
Muscle	0.23	
Fat	0.04	
Bone (Cortical)	0.02	
Bone (Cancellous)	0.08	
Cartilage	0.17	
Nerve	0.03	
Grey Matter	0.08	
White Matter	0.05	
Cerebellum	0.10	
CSF	2.00	
Vitreous Humor	1.50	
Lens	0.32	
Blood	0.70	

consists of 6 tissues: skin (layer between radius of 76-80 mm, with conductivity of 0.1 S/m), fat (74-76 mm, 0.04 S/m), muscle (72-74 mm, 0.23 S/m), skull (68-72 mm, 0.02 S/m), cerebrospinal fluid (66-68 mm, 2.0 S/m), and grey matter (0-66 mm, 0.08 S/m). The sphere is discretized with spatial resolutions of 0.5, 1, and 2 mm.

The Japanese adult male model, TARO, is the anatomical model considered in this study. The original TARO model, developed at NICT, Japan, consisted of 2-mm voxels [39], and a model with finer resolution was developed based on the algorithm proposed in [40].

The transverse section of a TARO at eye height is shown in Fig. 1 (b) and Table 1 lists the tissues in the head with their assigned conductivities [41]. The dosimetry is conducted for TARO's exposure to a 50 Hz, 0.1 mT uniform magnetic field oriented perpendicular to the coronal plane, that is, in the anterior-posterior (AP) vector direction.

C. POST-PROCESSING SCHEMES

With respect to ICNIRP's 2 mm × 2 mm × 2 mm averaging approach [2], Fig. 2 illustrates electric field averaging over a 2-mm cube for 1 mm and 0.5 mm voxels. The volume averaged *in situ* electric field, $E_V(\boldsymbol{r}_c)$, is evaluated as the arithmetic average of the vector electric field strength in the targeted tissue voxels in a 2-mm cube, and then assigned to the center voxel at $\boldsymbol{r}_c$. The volume of the targeted contiguous

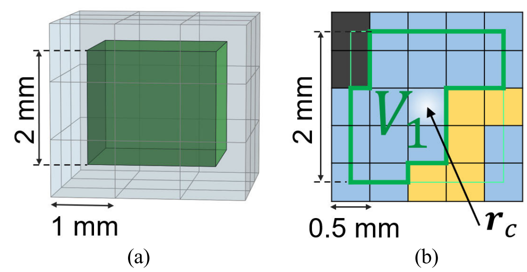

FIGURE 2. Demonstration of 2-mm cubic averaging: (a) intersection of averaging cube with voxels (res. = 1mm), (b) intersection of averaging cube with a contiguous tissue (res. = 0.5mm), outlined by thick green polygon. Voxels with different colors represent different tissues.

tissue inside the 2-mm cube is denoted by V_1, as outlined in thick green polygon in Fig. 2 (b). A factor, p, that represents the volume percentage of air/other tissues inside the 2-mm cube is defined as $p = 100 \times (V - V_1)/V$, where $V = 8$ mm^3. $p_{\max}$ is the maximum permissible percentage of air/other tissues in the cube. The averaging within target tissue ($\boldsymbol{r} \in V_1$) is performed using (2).

$$E_V(\boldsymbol{r}_c) = \begin{cases} \dfrac{1}{V_1}\left\| \sum\limits_{\boldsymbol{r}\in V_1} v(r)\boldsymbol{E}(\boldsymbol{r}) \right\|, & \text{if } p < p_{\max}, \\ 0\ \text{V/m}, & \text{otherwise,} \end{cases} \tag{2}$$

where $\boldsymbol{r}_c$ is the location of the cube center, $v(\boldsymbol{r})$ is the intersected volume of the 2-mm cube with the voxel centered at $\boldsymbol{r}(\boldsymbol{r} \in V_1)$. The volume-averaging is applied to all voxels each centered in their respective cubes. Note that the averaging is performed only for neighboring voxels within contiguous tissue. As illustrated in Fig. 2 (b), the two voxels in blue at the lower right corner of the 2-mm cube are not considered within V_1, even though they belong to the same tissue; however, the connectivity constraint is violated as shown in Fig. 2 (b). The connectivity of voxels is obtained using a three-dimensional two-way labelling method.

The IEEE standard [3] does not describe implementation of the 5-mm linear averaging it prescribes, nor does IEEE deal with tissue interfaces. A key reason is that IEEE uses ellipsoids rather than anatomical models for determining magnetic field coupling to tissue sites.

The scheme for evaluating 5-mm linear averaging for a targeted voxel at $\boldsymbol{r}_c$ is illustrated in Fig. 3 (a), in which a 5-mm averaging line is centered at the target voxel at $\boldsymbol{r}_c$, with its direction denoted by (θ, ϕ) in local spherical coordinates. Similar to the scheme for 2-mm cubic averaging, the ratio of air/other tissues is defined as $p = 100 \times (L - L_1)/L$, where L_1 is the length of the segment within the same tissue (illustrated in dark magenta in Fig. 3 (b)), and $L = 5$ mm. The thickness of the 5-mm averaging line is neglected, in consideration of the relatively large model resolution compared with the radius of a nerve axon. The linear averaging is performed using (3).

$$E_L(\boldsymbol{r}_c) = \begin{cases} \max\left(\dfrac{1}{L_1}\left\| \sum\limits_{\boldsymbol{r}\in L_1} l(\boldsymbol{r})\boldsymbol{E}(\boldsymbol{r}) \right\|\right), & \text{if } p < p_{\max}, \\ 0\ \text{V/m}, & \text{otherwise,} \end{cases} \tag{3}$$

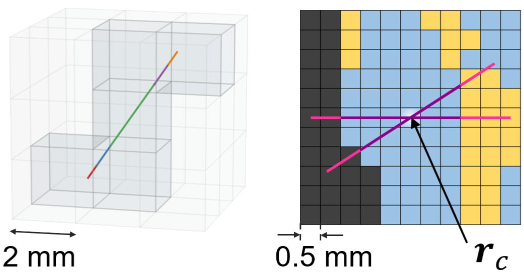

(a) (b)

FIGURE 3. Demonstration of 5-mm linear averaging: (a) intersection of the averaging line with tissue voxels (res. = 2mm), (b) intersection of the averaging line in different directions with tissue voxels (res. = 0.5mm). Voxels with different colors represent different tissues.

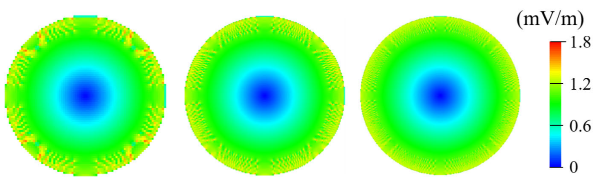

(a) (b) (c)

FIGURE 4. *In situ* electric field on the central cross section of the spherical model for uniform magnetic field exposure. Spatial resolution is (a) 2 mm, (b) 1 mm, and (c) 0.5 mm.

where $l(\boldsymbol{r})$ is the length of the intersected segment of the 5-mm line with the voxel centered at $\boldsymbol{r}$. Fig. 3(a) shows the 5-mm line intersecting with 5 contiguous voxels within the same tissue (resolution of 2 mm); each segment lengths shown in different colors in Fig. 3 (a) are calculated with the Liang–Barsky algorithm [42].

The directions of the averaging line (θ, ϕ) vary from 0° to 180° in 20° intervals. Averaging is performed over a total of 81 directions for the targeted voxel at $\boldsymbol{r}_c$. The final averaged value is taken as the maximum value over 81 records.

The relative difference in the averaged electric field between the volume- and line- averaging schemes is expressed as:

$$d_r = 100 \times \frac{|E_V - E_L|}{E_{\text{ref}}} \tag{4}$$

where the reference value, E_{ref}, is the mean of E_V and E_L.

III. COMPUTATIONAL RESULTS

A. MULTI-LAYER SPHERE

Fig. 4 shows the distributions of *in situ* electric field in the cross sections of the spherical model with different resolutions. The highest electric field strengths, as expected, are located at the model surfaces. The field distributions for all three resolutions are generally in good agreement, except for slight differences at the tissue/air and tissue/tissue interfaces. For resolutions of 0.5, 1, and 2 mm, the maximum voxel *in situ* electric fields in the skin were 1.598, 1.561, and 1.501 mV/m, respectively, while they were 1.447, 1.430, and 1.305 mV/m, respectively, in the grey matter. This tendency is in line with previous findings that the maximum electric field increases with improved model resolution [29]. The values for 0.5 mm resolution are approximately 27% (skin) and 40% (grey matter) larger than the theoretical maxima, 1.256 mV/m for skin, and 1.037 mV/m for grey matter.

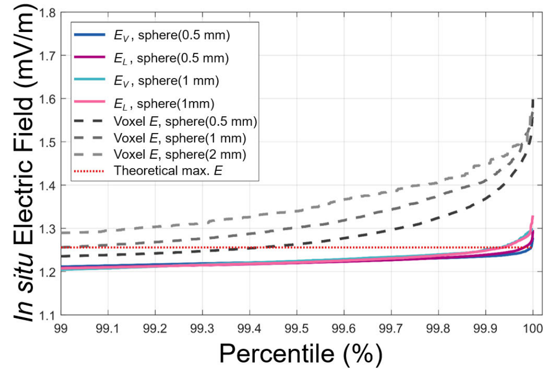

(a)

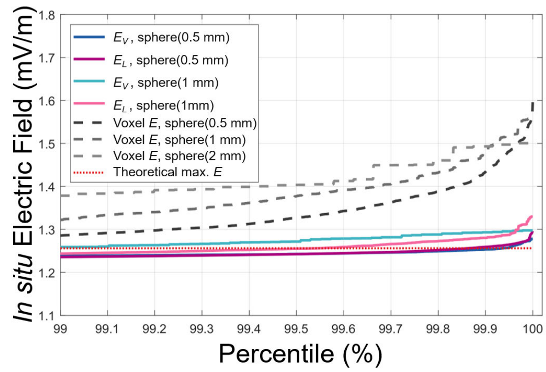

(b)

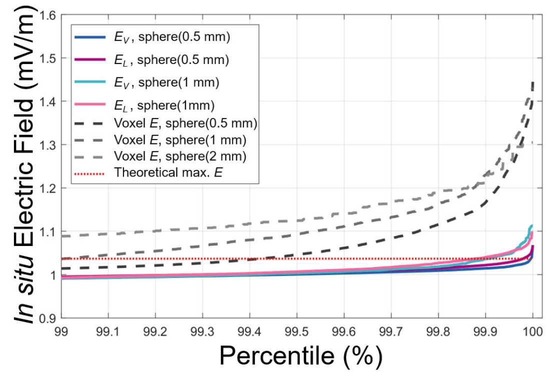

(c)

FIGURE 5. Percentile values of *in situ* electric field strength in 6-layered spherical model for (a) all tissues, (b) skin, and (c) grey matter ($p_{\max} = 0\%$).

Both averaging schemes were then applied to the *in situ* electric field strengths. The top 1% of the averaged field strengths are shown in Fig. 5. All tissues are represented in Fig. 5 (a), while skin and grey matter are shown separately in Figs. 5 (b) and (c), respectively ($p_{\max} = 0\%$ for all). In general, the percentile values of *in situ* electric field strength (excluding the maxima) are higher in the low-resolution models. This is because the highest electric field

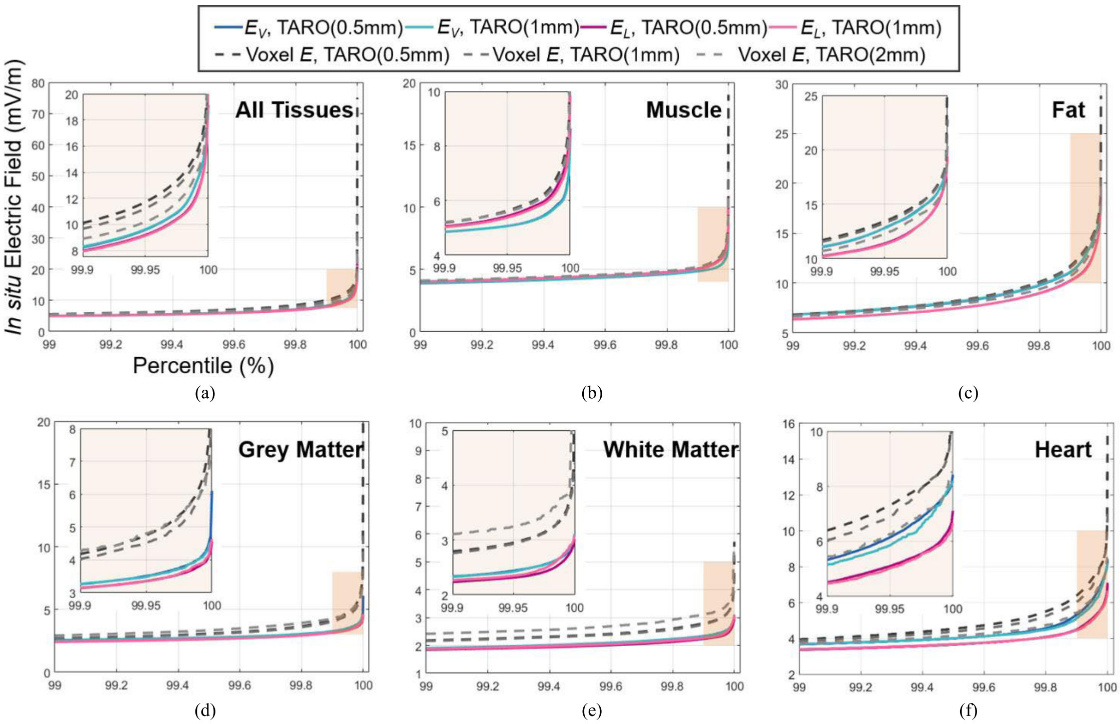

FIGURE 6. **Percentile values of volume-averaged, line-averaged, and voxel *in situ* electric field strength in TARO under uniform magnetic field exposure, for (a) all tissues, (b) muscle, (c) fat, (d) grey matter, (e) white matter, and (f) heart. Maximum permissible percentage for air/other tissues inclusion is $p_{\max} = 0\%$.**

strengths are at the surface of the sphere, and thus the lower-resolution sphere has a higher percentage of voxels near the tissue/air interface where artefacts are significant.

B. HUMAN BODY MODELS

The top 1% of the *in situ* electric field strengths in TARO are shown in Fig. 6. Fig. 6 (a) includes all tissues, and Figs. 6 (b)-(f) show each tissue individually. It is clear from this figure that both averaging schemes provide comparable results. In general, the higher resolution models have higher electric field strengths, except in the grey and white matter, which contain large areas of folded surfaces. This trend is different from that observed in the spherical model (Fig. 5), with the discrepancy attributable to the singularities originating from the complexity of the anatomical configurations of the human-like model. The line- and volume-averaged values are rather stable for different resolutions excluding the top ~0.1% voxels where computational artefacts could not be suppressed.

The volume-averaged, line-averaged, and voxel *in situ* electric field strengths on the surface of TARO are shown in Fig. 7. It is clear from this figure that the field distributions are similar to each other for models with different spatial resolutions. High electric field strengths can be observed around the neck, armpit and crotch regions, as expected.

C. DIFFERENCE BETWEEN TWO AVERAGING SCHEMES

The differences in the percentile values between the two averaging schemes are then investigated in terms of the relative differences defined by (4). The results are presented in Table 2 for the spherical model and in Table 3 for TARO.

For the spherical models, the relative differences between volume- and line-averaging (d_r) in the top 1% electric field are subtle; for $p_{\max} = 0\%$, they are $\leq 1.4\%$ for the model with a resolution of 0.5 mm, and $\leq 3.4\%$ for the model with a resolution of 1 mm (not shown). For the anatomical models, the largest relative difference is $\sim 30\%$ in the grey matter ($p_{\max} = 20\%$). If the highest 1% electric fields are excluded, the relative difference decreases to $\sim 3\%$ for muscle and white matter, and is less than 9% for fat and heart ($p_{\max} = 0\%$). Also for grey and white matter of TARO, d_r is low when $p_{\max} = 0\%$.

In order to clarify the difference between volume- and line- averaged electric fields, their spatial distributions are shown in Fig. 8. In Fig. 8 (a) and (b), all averaged voxels are compared. It is obvious that the differences between the two averaging schemes mainly exist on the tissue/air and tissue/tissue interfaces. This is because the sets of averaged voxels are different. For example, considering a targeted voxel located near a tissue boundary, a 2-mm cube-averaged field $E_V(\boldsymbol{r})$ might be 0 V/m, but the 5-mm line-averaged field $E_L(\boldsymbol{r})$ might be a non-zero value, and vice versa. In particular, the 2-mm cubic averaging excludes more voxels than the 5-mm linear averaging does. Also, tissues like the skin and retina are too thin to cover the whole 2 mm × 2 mm × 2 mm averaging volume, while the averaging line can be orientated such that the segment is still located within the same tissue. Marginal differences for both schemes can be observed from

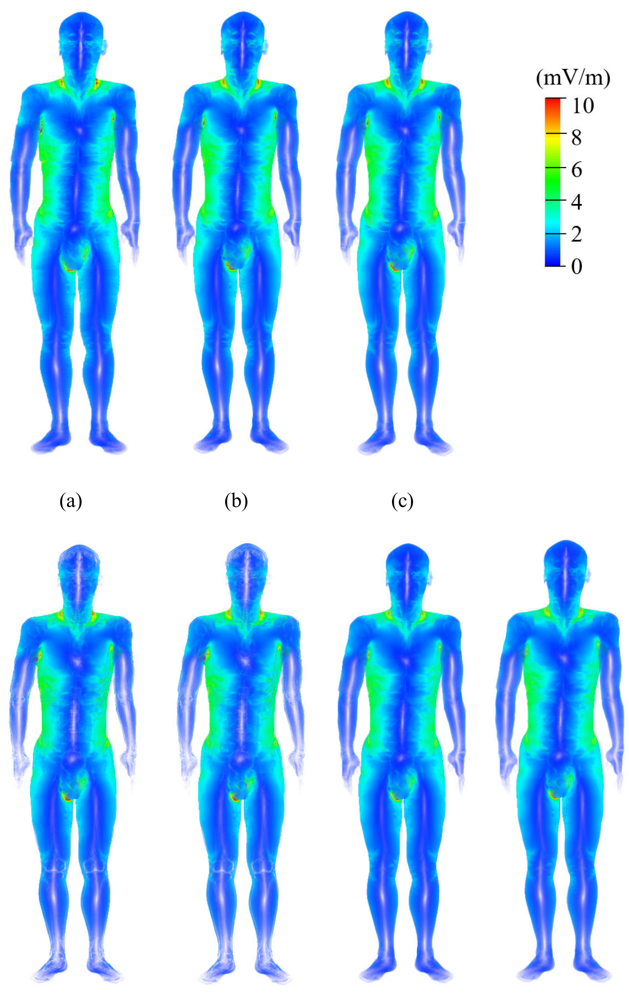

FIGURE 7. **Distributions of *in situ* electric field strength in TARO for uniform magnetic field exposure. Voxel field distributions are shown in (a), (b), and (c) for TARO with resolution of 2 mm, 1 mm, and 0.5 mm, respectively; volume-averaged field distributions are shown in (d) and (e) for TARO with resolution of 1 mm, and 0.5 mm, respectively; line-averaged field distributions are shown in (f) and (g) for TARO with resolution of 1 mm, and 0.5 mm, respectively. Maximum permissible percentage for air/other tissues inclusion is $p_{max} = 0\%$.**

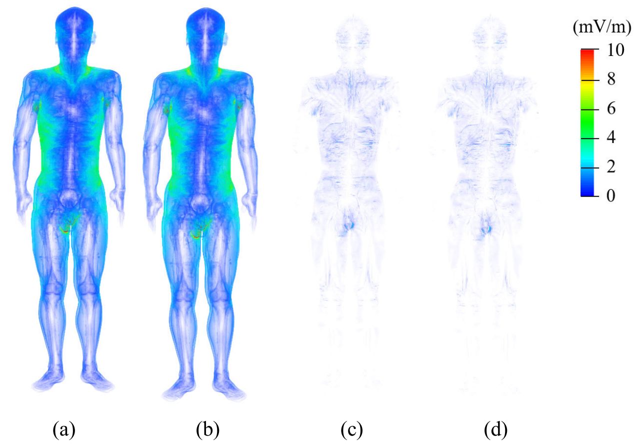

FIGURE 8. **Absolute differences in *in situ* electric field distributions between 5-mm line and 2-mm cubic averaging ($p_{max} = 0\%$). All voxels are included in (a) and (b) for TARO (res. = 1 mm) and TARO (res. = 0.5 mm) respectively; only common voxels are included in (c) and (d) for TARO (res. = 1 mm) and TARO (res. = 0.5 mm) respectively. The numbers of voxels in (c) and (d) are 69.7%, and 69.3% of those in (a) and (b), respectively.**

Fig. 8 (c) and (d), where only the averaged voxels in common for the two schemes are included.

D. AIR/OTHER TISSUES INCLUSION IN AVERAGING

With 2-mm cubic and 5-mm linear averaging, outermost layers of voxels of specific tissues are excluded from averaging, with more voxels excluded with finer resolution. We then investigated the *in situ* electric fields for different percentages of air/other tissues inclusion in the cube and line for post-processing.

Figs. 9 and 10 show the *in-situ* electric field strengths for different p_{max} values for the sphere and TARO, respectively. A value of $p_{max} = 0\%$ produces the lowest averaged *in situ* electric field. As p_{max} increases in steps of 10%, the percentile values increase toward the curves for voxel field strengths,

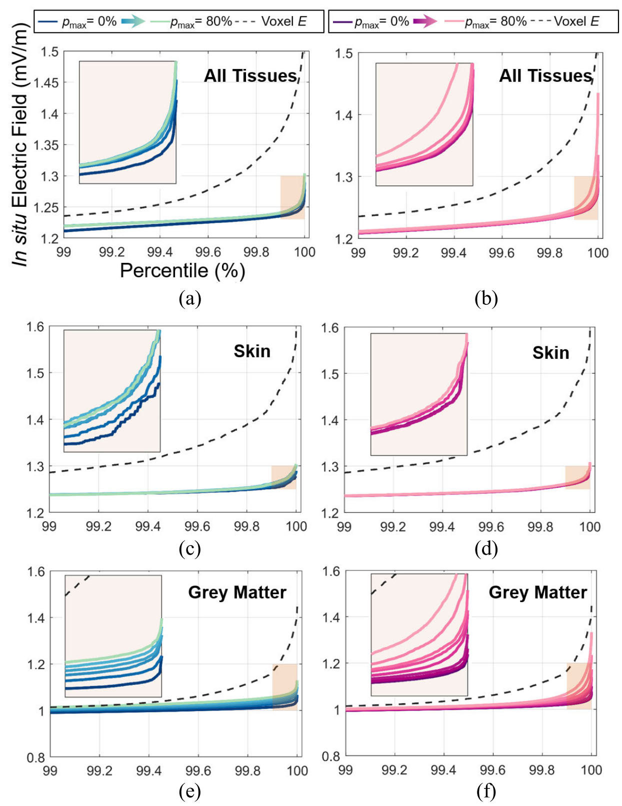

FIGURE 9. **Percentile values of volume-averaged, line-averaged, and voxel *in situ* electric fields in spherical model (res. = 0.5 mm) under uniform magnetic field exposure for different maximum permissible air/other tissues inclusions, left and right sub-figures represent volume-averaged and line-averaged results, respectively.**

and the relative differences between the two averaging are insignificant for the sphere and tend to decrease for TARO (Table 3). In general, with p_{max} set to >20-30%, reproducible

TABLE 2. Percentile values of *in situ* electric field strength in selected tissues of spherical model (Resolution of 0.5mm).

Tissue	Percentile (%)	$p_{max}=0\%$			$p_{max}=20\%$			$p_{max}=40\%$		
		E_V (mV/m)	E_L (mV/m)	d_r (%)	E_V (mV/m)	E_L (mV/m)	d_r (%)	E_V (mV/m)	E_L (mV/m)	d_r (%)
All Tissues	Max	1.28	1.30	1.4	1.30	1.30	0.5	1.30	1.30	0.6
	99.99	1.25	1.26	0.9	1.26	1.26	0.0	1.27	1.26	0.2
	99.9	1.24	1.24	0.3	1.24	1.24	0.1	1.24	1.24	0.1
	99	1.21	1.21	0.6	1.22	1.21	0.9	1.22	1.21	0.9
Skin	Max	1.28	1.30	1.4	1.30	1.30	0.5	1.30	1.30	0.6
	99.99	1.27	1.28	0.2	1.29	1.28	1.0	1.29	1.28	0.8
	99.9	1.25	1.26	0.5	1.26	1.26	0.1	1.26	1.26	0.1
	99	1.24	1.24	0.2	1.24	1.24	0.2	1.24	1.24	0.2
Grey Matter	Max	1.07	1.07	0.0	1.10	1.08	2.3	1.12	1.13	1.6
	99.99	1.03	1.04	1.3	1.06	1.05	1.6	1.08	1.08	0.0
	99.9	1.01	1.02	0.7	1.04	1.02	1.2	1.05	1.03	1.6
	99	0.99	0.99	0.4	1.00	1.00	0.7	1.01	1.00	1.2

TABLE 3. Percentile values of *in situ* electric field strength in selected tissues of TARO (Resolution of 0.5mm).

Tissue	Percentile (%)	$p_{max}=0\%$			$p_{max}=20\%$			$p_{max}=40\%$		
		E_V (mV/m)	E_L (mV/m)	d_r (%)	E_V (mV/m)	E_L (mV/m)	d_r (%)	E_V (mV/m)	E_L (mV/m)	d_r (%)
All Tissues	Max	19.14	23.86	21.9	30.62	26.12	15.9	30.62	32.13	4.8
	99.99	13.11	12.08	8.2	14.12	12.91	9.0	14.63	13.76	6.1
	99.9	8.25	7.98	3.3	9.28	8.39	10.1	9.77	9.04	7.8
	99	5.00	4.97	0.7	5.30	5.08	4.1	5.47	5.30	3.2
Skin	Max	-	23.86	-	30.62	26.12	15.9	30.62	32.13	4.8
	99.99	-	15.32	-	30.62	16.70	58.8	19.96	19.21	3.8
	99.9	-	9.80	-	29.44	10.56	94.1	12.45	12.01	3.6
	99	-	5.65	-	18.22	5.78	103.6	6.21	6.02	3.0
Muscle	Max	8.65	10.88	22.9	11.29	10.88	3.7	11.56	11.86	2.6
	99.99	5.86	6.57	11.4	6.38	6.59	3.2	6.65	6.64	0.2
	99.9	4.85	5.05	3.9	5.03	5.06	0.6	5.10	5.07	0.5
	99	3.89	4.02	3.2	4.01	4.02	0.4	4.05	4.03	0.5
Fat	Max	19.14	19.41	1.4	20.14	19.41	3.7	21.40	20.67	3.5
	99.99	15.74	14.59	7.6	15.96	15.17	5.0	16.01	15.57	2.8
	99.9	11.06	10.22	7.9	11.44	10.65	7.1	11.50	11.08	3.7
	99	6.82	6.34	7.3	6.82	6.48	5.1	6.79	6.65	2.2
Grey Matter	Max	6.10	4.56	29.0	7.34	5.40	30.5	8.49	7.34	14.5
	99.99	4.02	3.80	5.6	4.71	4.23	10.8	4.89	4.65	5.2
	99.9	3.26	3.14	3.7	3.59	3.34	7.2	3.68	3.58	2.8
	99	2.56	2.41	5.9	2.60	2.49	4.2	2.61	2.58	1.3
White Matter	Max	3.10	3.01	2.9	3.56	3.24	9.5	3.75	3.53	6.1
	99.99	2.70	2.60	3.7	2.99	2.81	6.4	3.09	2.98	3.6
	99.9	2.34	2.23	4.4	2.59	2.39	8.2	2.69	2.56	4.7
	99	1.90	1.85	2.8	2.08	1.96	6.1	2.13	2.06	3.3
Heart	Max	8.43	7.11	17.0	9.71	7.56	25.0	10.21	8.26	21.1
	99.99	7.49	6.00	22.0	7.92	6.98	12.5	7.99	7.58	5.3
	99.9	5.32	4.50	16.8	6.09	5.23	15.2	6.24	5.90	5.6
	99	3.68	3.37	8.6	3.87	3.56	8.3	3.90	3.80	2.6

results can be expected for TARO (Fig. 10). In contrast, the line-averaging appears more sensitive to p_{max}. This can be seen from the percentile values for the heart, where almost equally spaced curves are observed across p_{max}.

For relatively thin tissues such as skin, if $p_{max} = 0\%$, then all skin voxels are excluded from the cubic averaging. As seen from Fig. 10, $p_{max} \approx 30\%$ is required for 2-mm cubic averaging to generate stable percentile values (bottom curve). In contrast, 5-mm linear averaging is still reproducible even for thin tissue like the skin.

E. EFFECT OF THE AVERAGING CUBE SIZE

Table 4 and Table 5 summarize the calculated percentile values of the *in situ* electric fields in selected tissues for different sizes of averaging cubes for the sphere and for TARO, respectively, with 0.5 mm voxels and $p_{max} = 30\%$. In general,

TABLE 4. **Percentile values of *in situ* electric field strengths in selected tissues of sphere(0.5mm) for difference averaging cube size.**

Tissue	Percentile (%)	*In situ* electric field strength in mV/m (percentage difference with theoretical value)				
		Cube size=1mm	Cube size=1.5mm	Cube size=2mm	Cube size=2.5mm	Cube size=3mm
All tissues	Max	1.398(11.3%)	1.350(7.7%)	1.302(4.2%)	1.283(2.9%)	1.263(1.4%)
	99.99	1.313(4.6%)	1.289(3.1%)	1.263(1.2%)	1.256(0.9%)	1.245(0.1%)
	99.9	1.260(0.3%)	1.252(0.5%)	1.240(0.4%)	1.238(0.3%)	1.233(0.6%)
	99	1.223(2.6%)	1.221(0.4%)	1.219(0.4%)	1.218(0.4%)	1.218(0.3%)
Skin	Max	1.40(11.3%)	1.35(7.7%)	1.30(4.2%)	1.28(2.9%)	1.26(1.4%)
	99.99	1.35(7.8%)	1.32(5.4%)	1.29(2.9%)	1.28(2.4%)	1.26(1.1%)
	99.9	1.30(3.9%)	1.28(2.7%)	1.26(1.0%)	1.25(0.7%)	1.24(0.0%)
	99	1.25(0.4%)	1.25(0.2%)	1.24(0.5%)	1.24(0.4%)	1.23(0.6%)
GM	Max	1.22(17.2%)	1.16(12.3%)	1.10(7.0%)	1.09(6.0%)	1.06(3.3%)
	99.99	1.15(10.7%)	1.10(6.9%)	1.07(4.0%)	1.06(3.6%)	1.05(2.4%)
	99.9	1.07(3.0%)	1.06(3.0%)	1.04(1.8%)	1.04(1.7%)	1.03(1.2%)
	99	1.01(2.7%)	1.01(0.2%)	1.01(0.1%)	1.01(0.1%)	1.00(0.1%)

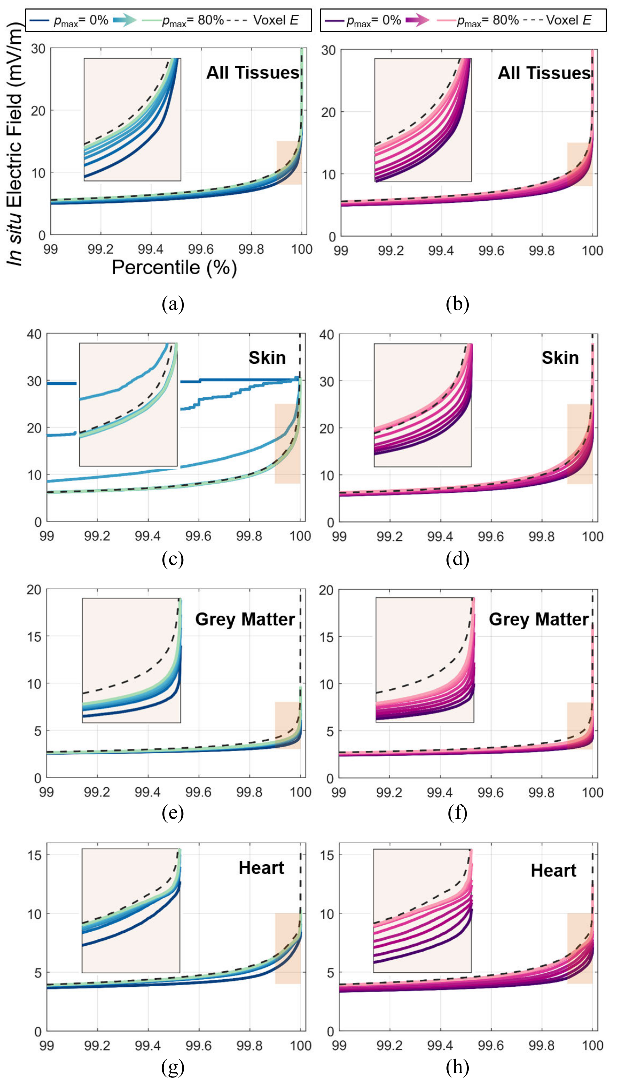

FIGURE 10. **Percentile values of volume-averaged, line-averaged and voxel *in situ* electric field strength in TARO (res. = 0.5mm) under uniform magnetic field exposure for different maximum permissible air/other tissues inclusions, left and right sub-figures represent volume-averaged and line-averaged results, respectively.**

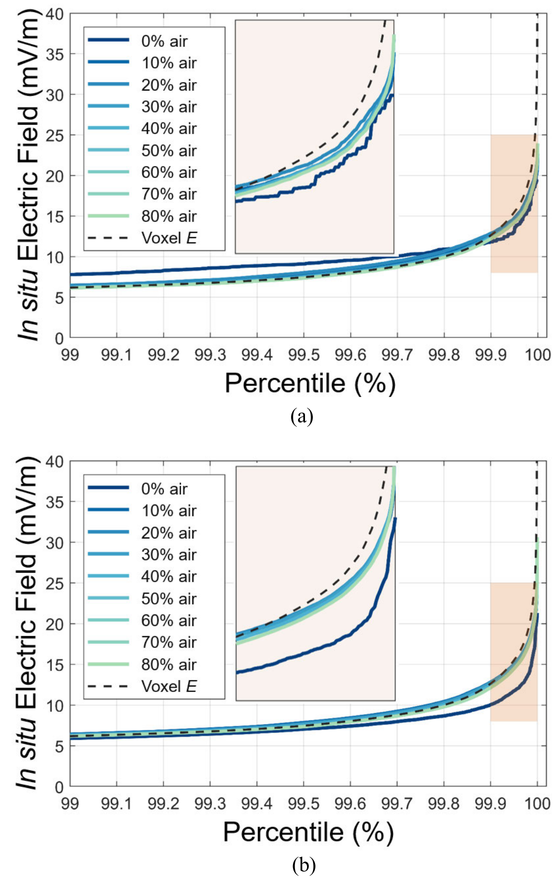

FIGURE 11. **Percentile values of volume-averaged and voxel *in situ* electric field strength in the skin of TARO with different ratios of maximum permissible percentage of air inclusion. Model resolution is (a) 1 mm, (b) 0.5 mm.**

for both models the averaged electric field strength decreases with cube size (except for skin in TARO). Specifically, the ratio of the maximum electric field strength averaged over 1-mm cube to that averaged over 3-mm cube is about 1.1, and 2, for the sphere and TARO, respectively, but for both models, the 99th to 99.99th percentile values are less dependent on the averaging volume.

For the spherical model, the relative differences between numerical and theoretical percentile values decrease slightly with the increased cubic size. Also, for the 99th to 99.99th

TABLE 5. Percentile values of *in situ* electric field strengths in selected tissues of TARO(0.5mm) for difference averaging cube size.

Tissue	Percentile (%)	*In situ* electric field strength (mV/m)				
		Cube size=1mm	Cube size=1.5mm	Cube size=2mm	Cube size=2.5mm	Cube size=3mm
All tissues	Max	45.60	40.08	30.62	29.29	22.43
	99.99	14.92	14.76	14.35	14.16	13.81
	99.9	9.89	9.78	9.54	9.38	9.07
	99	5.50	5.47	5.38	5.33	5.25
Skin	Max	45.60	40.08	30.62	29.29	22.43
	99.99	21.19	21.34	25.36	27.85	22.43
	99.9	12.43	12.89	17.25	25.29	22.19
	99	6.13	6.28	8.48	17.29	20.07
GM	Max	12.10	10.77	7.92	6.62	5.95
	99.99	5.36	5.18	4.81	4.63	4.35
	99.9	3.89	3.80	3.64	3.55	3.43
	99	2.66	2.64	2.61	2.59	2.56
Heart	Max	12.23	11.36	9.98	9.26	8.70
	99.99	8.22	8.14	7.96	7.86	7.73
	99.9	6.31	6.26	6.15	6.10	6.01
	99	3.92	3.92	3.89	3.88	3.85

results for TARO. Specifically, the 99th to 99.99th percentile values for grey matter and heart are fairly stable for different sizes of the cubes. Relatively large variability can be found in skin even for the 99th percentile values. This is because a larger averaging cube tends to exclude more skin voxels with a given $p_{\max}$.

F. INCLUSION OF SUBCUTANEOUS TISSUE IN VOLUME-AVERAGING FOR SKIN

For thin tissues like skin, the ICNIRP guideline (2010) suggests that the averaging volume "*may extend to subcutaneous tissue*" [2]. Inclusion of subcutaneous tissue in volume averaging for the skin was factored into this study by redefining V_1 in (2) as the volume of non-air voxels in a 2-mm cube. Consequently, for this case, the ratio $p_{\max}$ is redefined as the maximum permissible air inside the cube.

Figs. 11(a) and (b) show the calculated percentile *in situ* electric fields for the skin of the TARO models with a resolution of 1 mm and 0.5 mm, respectively. As can be seen, for $p_{\max} > 10\%$, the percentile values are clearly more stable than previously calculated (see Table 4). If no air voxels are allowed in the averaging cube (i.e. $p_{\max} > 0\%$), large variations are still observed.

IV. DISCUSSION AND CONCLUDING REMARKS

This study developed methods for implementing 2-mm cubic and 5-mm linear averaging of electric fields induced in tissue by magnetic fields as prescribed, respectively, by ICNIRP and IEEE. The ICNIRP guideline states, "*the $2 \times 2 \times 2$ mm^3 averaging volume should not extend beyond the boundary of the tissue except for tissues such as the retina and skin, which are too thin to cover the whole averaging cube.*" Aside from this stipulation, neither guideline provides further guidance as to specific dosimetric procedures for assessing compliance with the BR or DRL. The analyses presented here compare the induced *in situ* electric fields between the two averaging schemes over different voxel resolutions when the computational boundaries fall entirely within the specific target tissue (Fig. 6), and when spatial averaging is extended to computational boundaries that span a tissue/tissue or tissue/air interface (Fig. 10).

This paper first adopted the spherical model as a convenient way to demonstrate "*proof of concept*" concerning tissue inclusion, but given its shape regularity, its results do not represent the variability seen in the anatomical modeling across $p_{\max}$ (Tables 2 and 3) and cube size (Tables 4 and 5).

A previous study of dose to brain tissue from transcranial magnetic stimulation reported good agreement between the median *in situ* electric fields and corresponding 95% confidence intervals for both the 2-mm cubic and 5-mm linear averages of *in situ* electric fields [43]. The study in this paper reports a similar tendency (Table 3) for the $\leq$ 99.99th percentile of inner tissues, with relatively large differences for maximum values (100th percentile). These latter differences occur at voxels located at tissue boundaries as well as at skin-to-skin contact regions where stair-casing errors are not easily excluded by spatial averaging alone [32], [44]. Although cubic and linear averaging probably relate to different *in situ* electric field interactions, the dosimetry results indicate that their percentile *in situ* electric fields are not radically different from one another. Thus, neither scheme is likely to cause a significant difference between ICNIRP and IEEE with respect to dose estimation. Differences across populations – size, shape, tissue mix, etc. – and exposure scenario will probably produce more variability than the respective algorithms.

For all but muscle, the anatomical model results (Table 3) show slightly lower electric fields for linear than for cubic averaging. The reason is that the larger stencil dimension (the long dimension of the averaging line/volume, i.e., 5 mm vs. 2 mm) results in the tendency of the linear method's spatial filtering to yield lower electric field values, compared to cubic averaging. Below the 99th percentile, the 2-mm cubic and 5-mm linear averaged *in situ* electric fields were comparable (data not shown). A recent study [33] suggested that 99.99th percentile is a computationally stable metric for the same model using different numerical methods. Nonetheless, only limited data are available with which to recommend an optimal percentile estimate of maximum dose to tissue from magnetic field exposure.

Restricting the averaging computations to only those cubic volumes or linear segments completely within a tissue will very often lead to the exclusion of voxels located at the tissue boundaries. Consequently, both artefacts and actual physical fields are excluded by post-processing, and furthermore, more voxels are excluded with higher resolution models. Our results suggest that a percentage of air/other tissues may be included in post-processing as a practical compromise, accounting for more tissue and permitting higher resolutions, recognizing, however, that the additional anatomical volume or linear segment beyond the tissue boundary may not relate to the biological effect of interest (synaptic activity alteration or PNS). The results indicate that 2-mm cubic averaging provides stable post-processing percentiles with a ∼20% to ∼30% inclusion criterion for inner tissues. In contrast, 5-mm linear averaging is more sensitive to $p_{\max}$ (Fig. 10).

For cubic averaging in skin, a large variation of calculated *in situ* electric fields occurs if no air/other tissues are allowed in the computational volume (Fig. 10). As indicated in Results, ICNIRP permits extending into subcutaneous tissue when averaging for skin [2]. This is based on recognizing both skin and fat as surrogates for PNS, even without rigorous validation [45]. We suggest (subsection III.F) that for skin, at least ∼10% air inclusion is necessary for reproducibly averaged electric fields with different voxel resolutions, even when subcutaneous tissues are also included in the averaging (Fig. 11).

To recommend appropriate percentile values for *in situ* electric fields with the averaging schemes considered here will require further study.

REFERENCES

[1] International Commission on Non-Ionizing Radiation Protection, "Guidelines for limiting exposure to time-varying electric, magnetic, and electromagnetic fields (up to 300 GHz)," *Health Phys.*, vol. 74, no. 4, pp. 494–521, 1998.

[2] International Commission on Non-Ionizing Radiation Protection, "Guidelines for limiting exposure to time-varying electric and magnetic fields (1 Hz to 100 kHz)," *Health Phys.*, vol. 99, no. 6, pp. 818–836, 2010.

[3] *IEEE Standard for Safety Levels with Respect to Human Exposure to Electric, Magnetic and Electromagnetic Fields,* 0 *Hz to 300 GHz*. Standard IEEE-C95.1, New York, NY, USA, 2019.

[4] *IEEE Standard for Safety Levels with Respect to Human Exposure to Electromagnetic Fields,* 0 *to 3 KHz*, Standard IEEE-C95.6, New York, NY, USA, 2002.

[5] J. P. Reilly and A. Hirata, "Low-frequency electrical dosimetry: Research agenda of the IEEE International Committee on Electromagnetic Safety," *Phys. Med. Biol.*, vol. 61, no. 12, p. R138, 2016.

[6] V. De Santis and X. L. Chen, "On the issues related to compliance assessment of ICNIRP 2010 basic restrictions," *J. Radiol. Prot.*, vol. 34, no. 2, pp. 31–39, 2014.

[7] X. Chen, "Analysis of human brain exposure to low-frequency magnetic fields: A numerical assessment of spatially averaged electric fields and exposure limits," *Bioelectromagnetics*, vol. 34, no. 1, pp. 375–384, 2013.

[8] J. G. Jefferys, "Experimental neurobiology of epilepsies," *Current Opinion Neurol.*, vol. 7, no. 2, pp. 113–122, 1994.

[9] J. P. Reilly and A. M. Diamant, "Spatial relationships in electrostimulation: Application to electromagnetic field standards," *IEEE Trans. Biomed. Eng.*, vol. 50, no. 6, pp. 783–785, Jun. 2003.

[10] D. Poljak, M. Cvetković, O. Bottauscio, A. Hirata, I. Laakso, E. Neufeld, S. Reboux, C. Warren, A. Giannopoulos, and F. Costen, "On the use of conformal models and methods in dosimetry for nonuniform field exposure," *IEEE Trans. Electromagn. Compat.*, vol. 60, no. 2, pp. 328–337, Apr. 2018.

[11] J. Gomez-Tames, I. Laakso, Y. Haba, A. Hirata, D. Poljak, and K. Yamazaki, "Computational artifacts of the in situ electric field in anatomical models exposed to low-frequency magnetic field," *IEEE Trans. Electromagn. Compat.*, vol. 60, no. 3, pp. 589–597, Jun. 2018.

[12] J. P. Reilly, "Survey of numerical electrostimulation models," *Phys. Med. Biol.*, vol. 61, no. 12, pp. 4346–4363, 2016.

[13] A. Hirata, K. Caputa, T. W. Dawson, and M. A. Stuchly, "Dosimetry in models of child and adult for low-frequency electric field," *IEEE Trans. Biomed. Eng.*, vol. 48, no. 9, pp. 1007–1012, Sep. 2001.

[14] P. J. Dimbylow, "Induced current densities from low-frequency magnetic fields in a 2 mm resolution, anatomically realistic model of the body," *Phys. Med. Biol.*, vol. 43, no. 2, pp. 221–230, Feb. 1998.

[15] K. Wake, I. Laakso, A. Hirata, J. Chakarothai, T. Onishi, S. Watanabe, V. De Santis, M. Feliziani, and M. Taki, "Derivation of coupling factors for different wireless power transfer systems: Inter-and intralaboratory comparison," *IEEE Trans. Electromagn. Compat.*, vol. 59, no. 2, pp. 1–9, 2016.

[16] A. Hirata, Y. Takano, Y. Kamimura, and O. Fujiwara, "Effect of the averaging, vol. and, algorithm on the in situ electric field for uniform electric- and magnetic-field exposures," *Phys. Med. Biol.*, vol. 55, no. 9, pp. N243–N252, 2010.

[17] K. Yamazaki, M. Taki, and C. Ohkubo, "Safety assessment of human exposure to intermediate frequency electromagnetic fields," *Electr. Eng. Jpn.*, vol. 197, no. 4, pp. 3–11, 2016.

[18] Y. Diao, W. Sun, Y. He, S. W. Leung, and Y. M. Siu, "Equivalent magnetic vector potential model for low-frequency magnetic exposure assessment," *Phys. Med. Biol.*, vol. 62, no. 19, pp. 7905–7922, 2017.

[19] K. Taguchi, "Relationship of external field strength with local and whole-body averaged specific absorption rates in anatomical human models," *IEEE Access*, vol. 6, pp. 70186–70196, 2018.

[20] S. W. Park, "Evaluation of electromagnetic exposure during 85 kHz wireless power transfer for electric vehicles," *IEEE Trans. Magn.*, vol. 54, no. 1, Jan. 2018, Art. no. 5100208.

[21] F. Freschi, L. Giaccone, V. Cirimele, and A. Canova, "Numerical assessment of low-frequency dosimetry from sampled magnetic fields," *Phys. Med. Biol.*, vol. 63, no. 1, 2017, Art. no. 15029.

[22] T. Shimamoto, I. Laakso, and A. Hirata, "*In-situ* electric field in human body model in different postures for wireless power transfer system in an electrical vehicle," *Phys. Med. Biol.*, vol. 60, pp. 163–173, Dec. 2014.

[23] C. Li and T. Wu, "Dosimetry of infant exposure to power-frequency magnetic fields: Variation of 99th percentile induced electric field value by posture and skin-to-skin contact," *Bioelectromagnetics*, vol. 36, no. 3, pp. 204–218, 2015.

[24] T. W. Dawson and M. A. Stuchly, "High-resolution organ dosimetry for human exposure to low-frequency magnetic fields," *IEEE Trans. Magn.*, vol. 34, no. 3, pp. 708–718, May 1998.

[25] B. Kos, B. Valič, T. Kotnik, and P. Gajšek, "Induced electric fields in workers near low-frequency induction heating machines," *Bioelectromagnetics*, vol. 35, no. 3, pp. 222–226, 2014.

[26] M. A. Stuchly and O. P. Gandhi, "Inter-laboratory comparison of numerical dosimetry for human exposure to 60 Hz electric and magnetic fields," *Bioelectromagnetics*, vol. 21, no. 3, pp. 167–174, 2000.

[27] A. Hirata, K. Yamazaki, S. Hamada, Y. Kamimura, H. Tarao, K. Wake, Y. Suzuki, N. Hayashi, and O. Fujiwara, "Intercomparison of induced fields in Japanese male model for ELF magnetic field exposures: Effect of different computational methods and codes," *Radiat. Protection Dosimetry*, vol. 138, no. 3, pp. 237–244, Nov. 2010.

[28] K. Aga, "Intercomparison of in situ electric fields in human models exposed to spatially uniform magnetic fields," *IEEE Access*, vol. 6, pp. 70964–70973, 2018.

[29] T. W. Dawson, M. Potter, and M. A. Stuchly, "Evaluation of modeling accuracy of power frequency field interactions with the human body," *Appl. Comput. Electromagn. Soc. J.*, vol. 16, no. 2, pp. 162–172, 2001.

[30] A. Hirata, Y. Takano, O. Fujiwara, T. Dovan, and R. Kavet, "An electric field induced in the retina and brain at threshold magnetic flux density causing magnetophosphenes," *Phys. Med. Biol.*, vol. 56, no. 13, pp. 4091–4101, Jun. 2011.

[31] E. A. Rashed, J. Gomez-Tames, and A. Hirata, "Human head skin thickness modeling for electromagnetic dosimetry," *IEEE Access*, vol. 7, pp. 46176–46186, 2019.

[32] V. De Santis, X. L. Chen, I. Laakso, and A. Hirata, "An equivalent skin conductivity model for low-frequency magnetic field dosimetry," *Biomed. Phys. Eng. Express*, vol. 1, no. 1, 2015, Art. no. 15201.

[33] M. Soldati and I. Laakso, "Computational errors of the induced electric field in voxelized and tetrahedral anatomical head models exposed to spatially uniform and localized magnetic fields," *Phys. Med. Biol.*, to be published, doi: 10.1088/1361-6560/ab5dfb.

[34] I. Laakso and A. Hirata, "Reducing the staircasing error in computational dosimetry of low-frequency electromagnetic fields," *Phys. Med. Biol.*, vol. 57, no. 4, pp. 25–34, 2012.

[35] A. Hirata, F. Ito, and I. Laakso, "Confirmation of quasi-static approximation in SAR evaluation for a wireless power transfer system," *Phys. Med. Biol.*, vol. 58, no. 17, pp. 241–249, 2013.

[36] A. Barchanski, H. De Gersem, E. Gjonaj, and T. Weiland, "Impact of the displacement current on low-frequency electromagnetic fields computed using high-resolution anatomy models," *Phys. Med. Biol.*, vol. 50, no. 19, pp. N243–N249, 2005.

[37] S. W. Park, K. Wake, and S. Watanabe, "Calculation errors of the electric field induced in a human body under quasi-static approximation conditions," *IEEE Trans. Microw. Theory Techn.*, vol. 61, no. 5, pp. 2153–2160, May 2013.

[38] I. Laakso and A. Hirata, "Fast multigrid-based computation of the induced electric field for transcranial magnetic stimulation," *Phys. Med. Biol.*, vol. 57, no. 23, pp. 7753–7765, 2012.

[39] T. Nagaoka, "Development of realistic high-resolution whole-body voxel models of Japanese adult males and females of average height and weight, and application of models to radio-frequency electromagnetic-field dosimetry," *Phys. Med. Biol.*, vol. 49, no. 1, pp. 1–15, 2004.

[40] K. Taguchi, T. Kashiwa, and A. Hirata, "Development on high resolution human voxel model for high frequency exposure analysis," presented at the Prog. Electromagn. Res. Symp., Toyama, Japan, Aug. 2018.

[41] S. Gabriel, R. W. Lau, and C. Gabriel, "The dielectric properties of biological tissues: III. Parametric models for the dielectric spectrum of tissues," *Phys. Med. Biol.*, vol. 41, no. 11, pp. 2271–2293, 1996.

[42] Y.-D. Liang and B. A. Barsky, "A new concept and method for line clipping," *ACM Trans. Graph.*, vol. 3, no. 1, pp. 1–22, 1984.

[43] M. Soldati, M. Mikkonen, I. Laakso, T. Murakami, Y. Ugawa, and A. Hirata, "A multi-scale computational approach based on TMS experiments for the assessment of electro-stimulation thresholds of the brain at intermediate frequencies," *Phys. Med. Biol.*, vol. 63, no. 22, 2018, Art. no. 225006.

[44] G. Schmid, S. Cecil, and R. Überbacher, "The role of skin conductivity in a low frequency exposure assessment for peripheral nerve tissue according to the ICNIRP 2010 guidelines," *Phys. Med. Biol.*, vol. 58, no. 13, pp. 4703–4716, 2013.

[45] R. Kavet, T. Dovan, and J. P. Reilly, "The relationship between anatomically correct electric and magnetic field dosimetry and published electric and magnetic field exposure limits," *Radiat. Prot. Dosimetry*, vol. 152, no. 4, pp. 279–295, May 2012.

YINLIANG DIAO (S'12–M'17) received the B.E. degree from Chongqing University, Chongqing, China, in 2008, the M.S. degree in electronic engineering from the Beijing University of Posts and Telecommunications, Beijing, China, in 2011, and the Ph.D. degree in electronic engineering from the City University of Hong Kong, in 2016. Since 2017, he has been an Assistant Professor with South China Agricultural University, Guangzhou, China. In 2019, he joined the Department of Electrical and Mechanical Engineering, Nagoya Institute of Technology, as a Researcher. His current research interests include electromagnetic dosimetry modeling and electromagnetic compatibility.

JOSE GOMEZ-TAMES was born in Cartago, Costa Rica. He received the B.S. degree in electronics engineering from the Institute of Technology of Costa Rica, Cartago, Costa Rica, in 2007, and the M.S and Ph.D. degrees in medical system engineering from Chiba University, Chiba, Japan, in 2012 and 2015, respectively.

From 2007 to 2009, he was an Instructor with the Institute of Technology of Costa Rica. From 2015 to 2016, he was a Research Fellow of the Japan Society for the Promotion of Science in 2015. Since 2016, he has been a Research Assistant Professor and subsequently Research Associate Professor with the Nagoya Institute of Technology. He has authored more than 50 articles published in international journals and conference proceedings. His researches focus on computational bioelectromagnetics, neural engineering, and their biomedical applications.

Dr. Gomez-Tames was a recipient of the Monbukagakusho Research Scholarship, the JSPS Postdoctoral Fellowship, and the Young Scientist Award in URSI General Assembly and Scientific Symposium, Montreal, Canada, in 2017. He is a Working Group Chair of subcommittee of EMF Dosimetry Modeling of the IEEE International Committee on Electromagnetic Safety and a member of the Scientific Expert Group of the International Commission on Non-Ionizing Radiation Protection.

ESSAM A. RASHED (S'07–M'11–SM'19) received the B.Sc. degree in scientific computing and the M.Sc. degree in computer science from Suez Canal University, Ismailia, Egypt, in 1998 and 2002, respectively, and the Ph.D. degree in computer science from the University of Tsukuba, Tsukuba, Japan, in 2010. From 2010 to 2012, he was a Research Fellow of the Japan Society for the Promotion of Science (JSPS), University of Tsukuba, Japan. He served as an Assistant Professor with the Department of Mathematics, Faculty of Science, Suez Canal University, from 2012 to 2016. Since 2016, he has been promoting as an Associate Professor with Suez Canal University, Egypt, and The British University in Egypt, Egypt (on Secondment). He is currently a Research Associate Professor with the Nagoya Institute of Technology. His research interests are medical image processing, data analysis and visualization, deep learning, and pattern recognition. Dr. Rashed was a recipient of the Egyptian National Doctoral Scholarship, in 2006, the JSPS Postdoctoral Fellowship, in 2010, the JAMIT Best Presentation Award, in 2008 and 2012, and the Chairman Award from the Department of Computer Science, University of Tsukuba, in 2010. He served as a PI for several projects funded from Science and Technology Development Fund (STDF), Egypt.

ROBERT (ROB) KAVET (M'10–SM'16) was born in Brooklyn, NY, USA, in October 1944. He received the master's degrees in electrical engineering from Cornell University, in 1967, and in environmental health sciences from the Harvard School of Public Health, in 1972, and the Sc.D. degree in respiratory physiology from the Harvard School of Public Health, in 1977. He has been involved with EMF health and safety issues since first joining the Electric Power Research Institute (EPRI) as a Project Manager, in 1978. Since 1978, he has been serving for a total of nearly 30 years at EPRI, retiring in 2016 as a Senior Technical Executive. His career at EPRI was committed to managing, designing, and participating in EMF health and safety research spanning the nonionizing spectrum from direct current (DC) through power frequencies to radio frequencies (RF). He is currently with the Harvard T. H. Chan School of Public Health, Boston, as a Visiting Scientist. He was involved intimately with studies that included the areas of epidemiology, exposure assessment, laboratory studies (in vivo and in vitro), dosimetry, instrumentation, and the development of modeling software. These studies covered key health and safety endpoints including cancer and pregnancy outcome, and the basis for exposure limits as published by the International Commission on Non-Ionizing Radiation Protection and IEEE. He has authored or coauthored about 100 peer-reviewed publications concerned with the above-mentioned EMF topics. Dr. Kavet is currently serving as a Co-Chair of subcommittee three of IEEE's International Committee on Electromagnetic Safety (ICES) concerned with establishing exposure standards for frequencies between 0 and 5 MHz.

AKIMASA HIRATA (S'98–M'01–SM'10–F'17) received the B.E., M.E., and Ph.D. degrees in communications engineering from Osaka University, Suita, Japan, in 1996, 1998, and 2000, respectively.

From 1999 to 2001, he was a Research Fellow with the Japan Society for the Promotion of Science, and also a Visiting Research Scientist with the University of Victoria, Victoria, BC, Canada, in 2000. In 2001, he joined the Department of Communications Engineering, Osaka University, as an Assistant Professor. In 2004, he joined, as an Associate Professor with the Department of Computer Science and Engineering, Nagoya Institute of Technology, where he is currently a Full Professor. His research interests include electromagnetic safety, risk management system for heat-related illness, methods in neuroscience, antennas, filters, and related computational techniques.

Prof. Hirata is an Editorial Board Member of physics in medicine and biology, a member of the main commission and a Chair of Project Group of the International Commission on Non-Ionizing Radiation Protection, and a member of administrative committee and a Subcommittee (EMF Dosimetry Modeling) Chair of the IEEE International Committee on Electromagnetic Safety, and an Expert of the World Health Organization. He is a Fellow of Institute of Physics and IEICE, and a member of IEE Japan and Bioelectromagnetics Society. He received several awards including Young scientists' Prize, in 2006 and Prizes for Science and Technology (Research Category 2011, Public Understanding Promotion Category 2014) by the Commendation for Science and Technology by the Minister of Education, Culture, Sports, Science, and Technology, Japan, the IEEE EMC-S Technical Achievement Award, in 2015, and the Japan Academy Medal and JSPS Prize, in 2018. From 2006 to 2012, he was also an Associate Editor of the IEEE TRANSACTIONS ON BIOMEDICAL ENGINEERING.